Investigation of magnetic journal bearing instability issues for MMR condition

Dokyu Kim [a], SeungJoon Baik [b], Jeong Ik Lee [a*]
aDepartment of Nuclear and Quantum Engineering, KAIST, Daejeon, South Korea
b Korea Atomic Energy Research Institute, Daejeon, South Korea
Corresponding author : jeongiklee@kaist.ac.kr

1. Introduction

The attention on the distributed power generation with nuclear energy is increasing due to the electricity grid decentralization and demand for mobile power generation without emission of CO_2. A concept of fully modularized fast reactor with a supercritical CO_2 (S-CO_2) cooled direct Brayton cycle, namely Micro Modular Reactor (MMR), is developed for 10MWe power output. Furthermore, MMR is being investigated for the potential application to substitute a diesel engine of a ship due to newly released International Maritime Organization, IMO regulation [1] .

In the proposed MMR, an appropriate bearing technology for turbomachinery is required. First, the MMR turbomachinery should be designed to be hermetic type because lubrication fluid bearings such as hydrodynamic oil or hydrostatic type is forced to add oil supply and sealing system that complicates the system. However, gas foil type does not have enough load capacity for MMR turbomachinery. Therefore, a magnetic type is a proper choice for MMR turbomachinery. This can be readily supported by the previous research [2] and Fig. 1.

Fig. 1. Bearing options for S-CO_2 Brayton Cycles for various power scales [2]

However, an instability issue for magnetic bearing was repeatedly mentioned under high speed operation and S-CO_2 conditions. With this instability, the shaft imbalance can grow until the clearance between the shaft and stator disappears leading to a crash. Shaft orbit regarding this issue is shown in Fig. 2. On the other hand, much higher speed operating in air condition does not have the same issue as shown in Fig. 3.
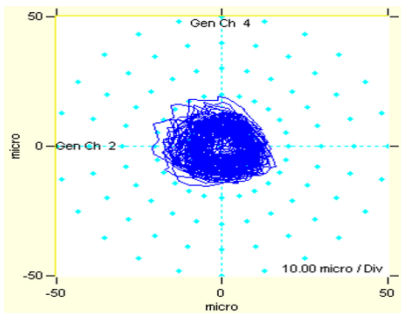

Fig. 2. Shaft center orbit at 14,000rpm, 43°C, 78 bar under S-CO_2 condition
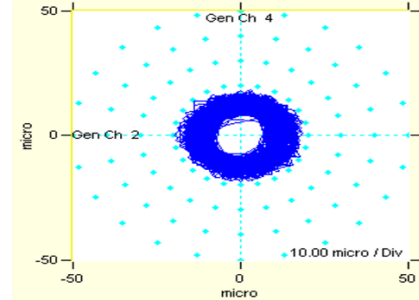

Fig. 3. Shaft center orbit at 30,000rpm under air condition

In this paper, the interaction between S-CO_2 lubricating fluid and magnetic bearing geometry is modeled to calculate the pressure distribution around the shaft. The calculation results from S-CO_2 conditions is compared to the other condition for analyzing the source of instability. From the discussion of the developed model, the instability source is predicted and the magnetic bearing experiment is exerted to verify the prediction and specify the instability source.

2. Methods and Results

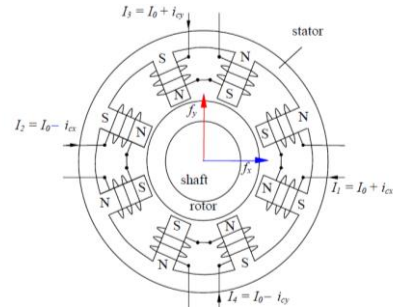### 2.1 Lubrication analysis for flow induced force on shaft

Fig. 4. Electromagnets in the magnetic bearing [3]

Active-control magnetic bearing (AMB) levitates the rotating shafts with electromagnets to apply magnetic force. The force from an electromagnet is expressed as in eq. (1). The AMB used for the experiments has 8 electromagnets as shown in Fig. 4. The empty space in Fig. 4 is filled with the working fluid. The spaces between the electromagnets potentially can generate a vortex and it can destabilize the shaft. Therefore, the experiments are planned to identify the effect of complex geometry by comparing 2 experiments. One is a test without any action for complex geometry and the other is a test with inner-coated AMB.

$$f = \frac{B^2 A_g}{2\mu_0} = \frac{\mu^2 N^2 I^2 A_g}{2\mu_0 l_g^2} \qquad (1), [3]$$

The fluid force is caused by pressure distribution around the shaft. In the 2nd test case, Reynolds equation is an appropriate governing equation (2) to obtain this distribution. It can be given by substituting the velocity profile from Navier-Stokes equation to the continuity equation for thin film. The geometry is described in Fig.5.

$$\frac{\partial}{\partial X}\left(\frac{\rho h^3}{12\mu}\frac{\partial p}{\partial X}\right) + \frac{\partial}{\partial Y}\left(\frac{\rho h^3}{12\mu}\frac{\partial p}{\partial Y}\right) = \frac{\partial(\rho h)}{\partial t} + \frac{1}{2}\left(\frac{\partial(\rho h u)}{\partial X} + \frac{\partial(\rho h v)}{\partial Y}\right) \quad (2), [4]$$

(Y : axial direction, t : time, v : axial velocity, u : circumferential velocity, ρ : density, μ : viscosity. The X'-Z' frame from Fig. 6 is denoted as X-Z frame for convenience.)
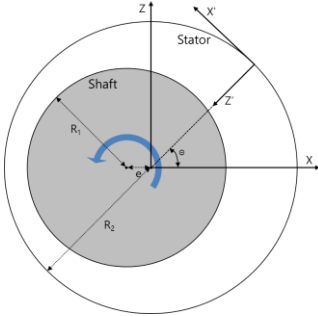

Fig. 5. Geometry of the unbalanced shaft and the stator

In this research, the Y direction is assumed to be negligible because the v is relatively smaller than the u. In addition, the transient term is removed to consider the steady state condition only. Therefore, (2) can be simplified as equation (3) with turbulence model which is described in Table I [5]. This is numerically solved by finite difference method (FDM) as shown in Fig. 6. This analysis model will be adapted for the described range as summarized in Table II.

$$\frac{\partial}{\partial X}\left(\frac{\rho h^3}{k_x\mu}\frac{\partial p}{\partial X}\right) = \frac{1}{2}\left(\frac{\partial(\rho h u)}{\partial X}\right) \quad (3)$$

($k_x = 12 + K_x Re^{n_x}$, : Reynolds number)

Table I. Coefficient in Ng-Pan model

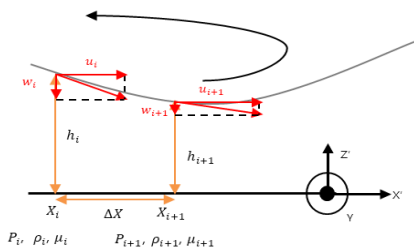| Reynolds number, Re	K_x	n_x
50,000<Re	0.0388	0.8
5000< Re <50000	0.0250	0.84
Re <5000	0.0039	1.06

Fig. 6. Coordinate description of Reynolds equation

Table II. Operation condition range of the model

Supply temperature	10 ~ 50 °C
Supply pressure	1 ~ 100bar
Rotational speed	30000 RPM
Eccentricity, ε = e/(R$_2$ − R$_1$)	0.07

The modeling results are shown with the fluid force for various thermal properties as Fig. 7 and 8.
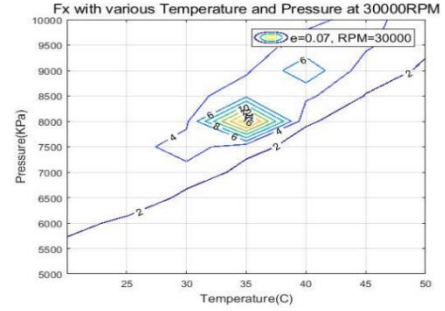

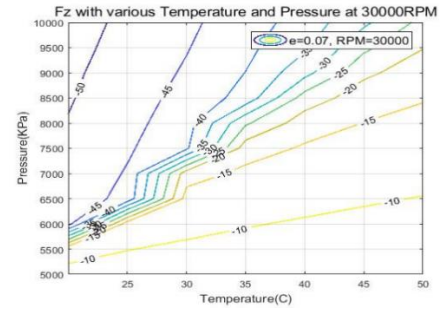Fig. 7. F_x contour, 30000RPM, ε=0.07

Fig. 8. F_z contour, 30000RPM, ε=0.07

Based on equation (3), the results are assumed to be the phenomena based on the density change or high density. Therefore, the analysis for air condition with high density & pressure and atmospheric condition were also evaluated for comparison. For the evaluation, the right hand side (RHS) of the equation is separated like (4).

$$\frac{\partial}{\partial X}\left(\frac{\rho h^3}{k_x\mu}\frac{\partial p}{\partial X}\right) = \left(\frac{hu}{2}\right)\frac{\partial \rho}{\partial X} + \left(\frac{u}{2}\frac{\partial h}{\partial X}\right)\rho \quad (4)$$

The first term of the RHS around the shaft is plotted in Fig. 9 and the second term is shown in Fig. 10. From these figures, it is concluded that the significant difference between the high density air and the S-CO$_2$ condition is caused by the first term of RHS in (4). Total values of the RHS around the shaft is plotted in Fig. 11. The integration of (4), $\frac{\rho h^3}{k_x\mu}\frac{\partial p}{\partial X}$ is plotted in Fig. 12 and the specific pressure distribution is shown in Fig. 13. The forces calculated from this distribution is organized as Table III. From Table III, it is concluded that the density changes induce F_x to become larger. This also explains the tendencies from Fig. 8
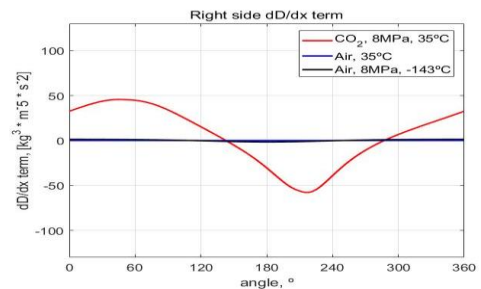

Fig. 9. $\left(\frac{hu}{2}\right)\frac{\partial \rho}{\partial X}$ around the shaft, ε = 0.25 and 30,000 RPM
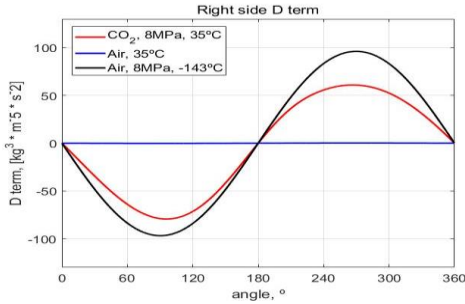
Fig. 10. $\left(\frac{u}{2}\frac{\partial h}{\partial X}\right)\rho$ around the shaft, $\boldsymbol{\varepsilon} = 0.25$ and 30,000 RPM
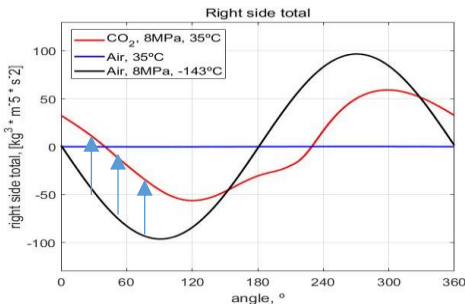

Fig. 11. RHS total around the shaft, $\boldsymbol{\varepsilon} = 0.25$ and 30,000 RPM
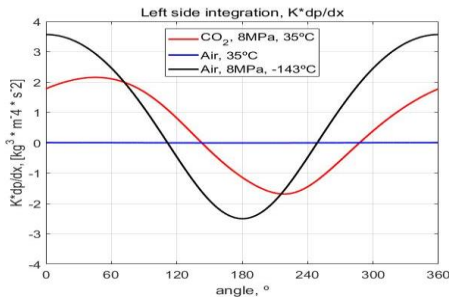

Fig. 12. $\frac{\rho h^3}{k_x \mu}\frac{\partial p}{\partial X}$ around the shaft, $\boldsymbol{\varepsilon} = 0.25$ and 30,000 RPM
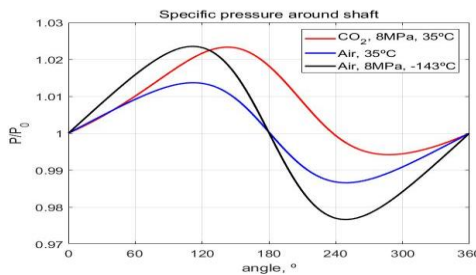

Fig. 13. Pressure distribution around the shaft, $\boldsymbol{\varepsilon} = 0.25$ and 30,000 RPM

Table III. Force on the shaft, $\boldsymbol{\varepsilon} = 0.25$ and 30,000 RPM

Thermal condition	F_x (N)	F_z (N)
Air at 0.1 MPa, 35 ℃	0.021	-1.852
Air at 8 MPa, -143 ℃	0.854	-256.4
CO_2 at 8 MPa, 35 ℃	100.8	-124.5

2.3 Experimental analysis of magnetic bearing instability

During the experiment, the CO_2's thermal state should be controlled. S-CO_2 pressurizing experiment (S-CO_2PE) facility will be used for this purpose. The magnetic bearing test rig is attached to this facility as shown in Fig. 15. The AMB test rig consists of the compressor and the AMB. The impeller is removed so only the bearing effect is expected to be dominant.
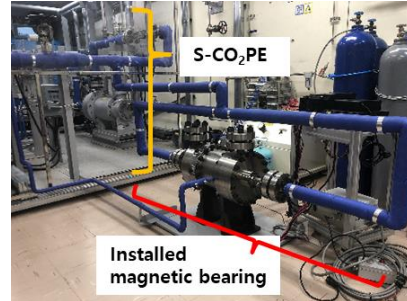

Fig. 15. The AMB & compressor system for S-CO_2

The experimental results will be analyzed from the measured shaft trajectory by inductive displacement sensor and the electric currents flows into the AMB. This trajectory is dynamically analyzed so the net force, F_{net} on the shaft will be calculated. This net force can be classified into three types; force from the lubricating fluid, F_{LUB}, AMB, F_{MB} [3] and the rotation of the unbalanced mass, F_{UB} [6]. The forces from other parts like labyrinth seal will be examined whether it is considerable or not. This is described with free body diagram as shown in Fig. 16.
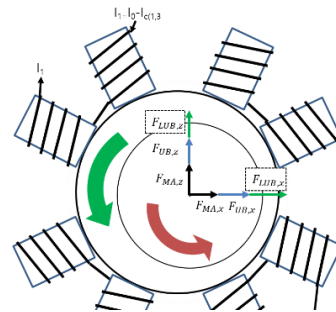

Fig. 16. Free body diagram of the shaft under AMB control

F_{MB} can be calculated with equation (1) and F_{UB}'s magnitude can be calculated as $U\omega^2$ (U : balance, unbalanced mass * distance between unbalance mass and center of the shaft). The direction of it with high speed rotation is verified as opposite of position. By subtract them from F_{net}, F_{LUB} can be obtained.
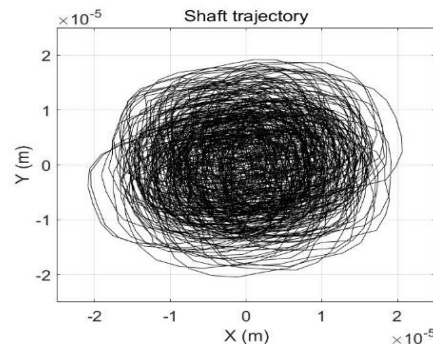

Fig. 17. Shaft trajectory data from S-CO_2 test and 30,000 RPM

The tests are proceeded with various RPM with 8 MPa & 36 ℃, (350kg/m^3) and no inner coating is possible. The shaft trajectory as shown in Fig. 17, it is observed that the shaft motion does not keep single revolving center when the RPM increases. Therefore, the direction of F_{UB} is obtained by tracing changed revolution center for each periods.

From these data, F_{LUB} is calculated. The force magnitudes for various eccentricities during the rotating operation are presented at Fig. 18. The F_{LUB} is larger than the lubrication model prediction. Because the significant difference between the model and the experiments is in geometry as mentioned in 2.1, the lubrication model results with 5 times and 25 times of the turbulence intensity are also included in these figures to illustrate the turbulence effect due to non-ideal geometry.
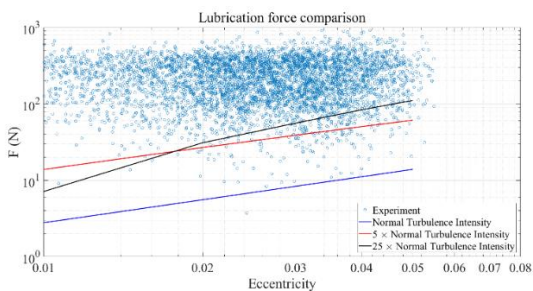

Fig. 18. F_{LUB} with 30,000 RPM ($K_x Re^{n_x}$: Turbulence intensity)

However, the phase is hard to analyze because the test results have many disturbances as shown in Fig. 19. Because it changed rapidly, Fourier transform is used to analyze it and one of the results are presented in Fig. 20
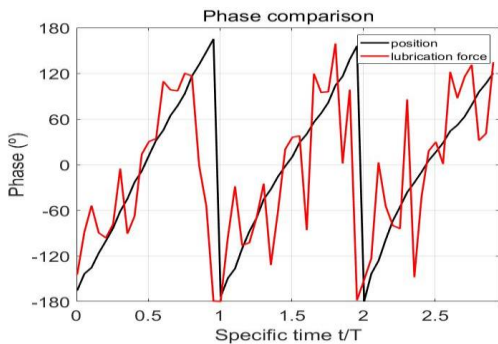

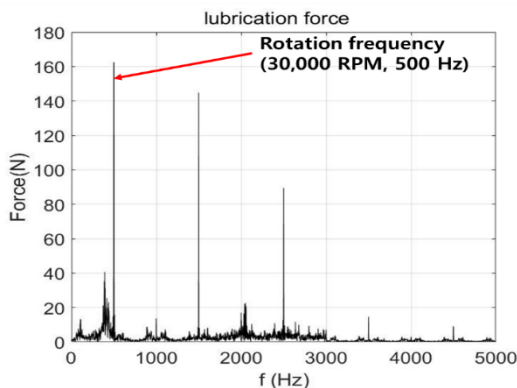Fig. 19. Phase data of F_{LUB} from S-CO$_2$ test 1 and 30,000 RPM

Fig. 20. Fourier transform data of F_{LUB} with 30,000 RPM

3. Conclusions

From the developed lubrication model, the instability source was predicted and magnetic bearing experimental system is constructed. The test with various RPM were performed for verifying the model and the instability sources. The comparison between the model and the tests shows that the model significantly under predicts the experimental data. Therefore, the model modification is necessary and it is left as the future work.

The lubrication force shows high frequency component that can cause instability. To analyze this, heat transfer model is planned to be incorporated to the lubrication model. In addition, the infinitesimal displacement model will be developed so that the lubrication model can correctly reflect the velocity terms.

The test with coated magnetic bearing is planned to commence in the near future. From this test, it is expected that the lubrication effects with close to ideal geometry can be finally compared fairly. By implementing these processes, the unstable operating region will be defined and the required performance of the AMB will be determined. From the modified model, dynamics of the shaft will be established for several different conditions. The trajectory of the shaft can be obtained from data and can be compared to the transient analysis of the rotor. If the model is well validated, this model can be adapted to MMR with transient operation. After developing an accurate model, the control logic of the magnetic bearing can be finally suggested.

REFERENCES

[1] Kim, S. G., Yu, H., Moon, J., Baik, S., Kim, Y., Jeong, Y. H., and Lee, J. I. (2017) A concept design of supercritical CO2 cooled SMR operating at isolated microgrid region. Int. J. Energy Res., 41: 512–525. doi: 10.1002/er.3633.
[2] Sienicki, James J., et al. "Scale dependencies of supercritical carbon dioxide Brayton cycle technologies and the optimal size for a next-step supercritical CO2 cycle demonstration." *SCO2 power cycle symposium*. 2011.
[3] Shelke, Santosh. "Controllability of Radial Magnetic Bearing." *Procedia Technology* 23 (2016): 106-113.
[4] Hamrock, Bernard J., Steven R. Schmid, and Bo O. Jacobson. *Fundamentals of fluid film lubrication*. CRC press, 2004.
[5] Taylor, C. M., and D. Dowson. "Turbulent lubrication theory—application to design." *Journal of Lubrication Technology* 96.1 (1974): 36-46.
[6] Muszynska, Agnieszka. Rotordynamics. CRC press, 2005